Practical calculations of the Aharonov-Bohm effect

1989 J. Phys. A: Math. Gen. 22 5195

(http://iopscience.iop.org/0305-4470/22/24/010)

J. Phys. A: Math. Gen. **22** (1989) 5195-5216. Printed in the UK

Practical calculations of the Aharonov–Bohm effect

G N Afanasiev and V M Shilov

Laboratory of Theoretical Physics, Joint Institute for Nuclear Research, Dubna, Moscow District, 141980 USSR

Received 20 December 1988

Abstract. We have found the scattering cross sections on two solenoids with opposite magnetic fluxes and on the toroidal solenoid in the presence or absence of a magnetic field. From this we extract the diffraction pattern shift which is due to the presence of the magnetic flux inside the solenoids. Practical recommendations for the performance of the experiments are given. It is proved that the crucial experiment on the existence of the AB effect suggested earlier could indeed be realised in practice.

1. Introduction

It is known that in multiconnected spaces non-equivalent representations of the angular momentum are permissible (see e.g. [1] and many references in [2-5]). Theory says that the Aharonov-Bohm (AB) effect exists for those representations to which single-valued wavefunctions correspond (see papers by Yang (pp 5-9), Aharonov (pp 10-19) in [2] and Ohnuki (pp 117-26) in [3]). Otherwise the effect does not exist [4]. The lack of theoretical justification for choosing one of these representations has recently given rise to numerous theoretical discussions (see e.g. [5]). Due to this theoretical uncertainty experiments testing the existence of the AB effect acquire decisive meaning. The shift of the diffraction pattern associated with the presence of the magnetic field was observed in experiments [6] in which electrons were scattered off a cylindrical solenoid. However, there are at least three factors which prevent unambiguous interpretation of these results. First, the finite length of the real cylindrical solenoid leads to magnetic field leakages near its ends. This allows one to attribute the positive outcomes of the above experiments to particle scattering on the magnetic field tails [7]. Another complication is due to the magnetic return flux of the cylindrical solenoid. It turns out [8] that the scattering cross section on this return flux exactly coincides with the AB one [9]. Third, the long-range behaviour of the vector potential for the cylindrical solenoid makes a unique separation of the complete wavefunction into the incoming and scattered ones impossible. From this numerous paradoxes arise [10].

More promising seem to be experiments in which electrons are scattered on magnetic field configurations lacking the above-mentioned shortcomings. The simplest magnetic fields of this kind are the magnetic field of the toroidal solenoid and that of two cylinders with opposite magnetic fluxes. In the experiments of Tonomura *et al* [11] electrons were scattered on the almost impenetrable toroidal potential barrier with a toroidal solenoid inside it. The shift of the diffraction pattern has been observed when the magnetic flux inside this solenoid was present. There exists the following qualitative interpretation of this shift. Consider two points P and P'. Continue the wavefunction from P to P' along different paths 1 and 2. The wavefunction gets different phase

0305-4470/89/245195+22$02.50

factors if inside the combined contour composed of paths 1 and 2 there is a non-vanishing magnetic flux. This is inconsistent with the single-valuedness of the wavefunction (which we suppose always to be fulfilled). Particular terms of the sum occurring in Feynman path-integral approach indeed acquire these factors. But this method itself, applied to the scattering in multiconnected regions, meets [12] with the ambiguities mentioned at the beginning of this section. Finally, we note that there is no known path-integral formulation for the toroidal solenoid.

We should like to mention [13, 14] in which the scattering amplitude f_m on the magnetic field ($\boldsymbol{H} = \text{rot}\,\boldsymbol{A} = 0$, but $\boldsymbol{A} \neq 0$) surrounding the toroidal solenoid (we call it the magnetic scattering amplitude or MSA for brevity) was obtained in the framework of Fraunhöfer diffraction theory. The measured cross section is, however, determined by the absolute square of the total scattering amplitude f. The latter is the sum of the scattering amplitude f_0 on the impenetrable potential barrier surrounding the solenoid and the magnetic scattering amplitude f_m: $f = f_0 + f_m$. The easiest way to check this is to write out the Lippmann-Schwinger equation in a form appropriate for the treated problem. This was done in [14].

Thus we intend to calculate the scattering cross section on the potential barrier without magnetic field ($\sigma_0 = |f_0|^2$) and with it ($\sigma = |f_0 + f_m|^2$), find from them the diffraction pattern shift and compare it with the experimental one. The plan of our exposition is as follows. In sections 2 and 3 we apply the Fraunhöfer diffraction theory to the evaluation of the electron cross sections on a toroidal solenoid and on two cylindrical solenoids with opposite magnetic fluxes. In section 4 we analyse the obtained diffraction patterns in detail, find the positions of maxima and minima of the cross sections and their shift arising from the magnetic field switching. We analyse under what conditions the experiment on existence of the AB effect proposed recently in [15] could be realised. The calculations presented justify theoretical predictions according to which the hidden fields (such as the magnetic field inside the solenoid) may lead to the disappearance of the probability and current densities in the accessible space regions. Turning to the experiments of Tonomura *et al* we find that Fraunhöfer diffraction describes them only quantitatively. The quantitative description is obtained in the framework of Fresnel diffraction theory. We apply this to the electron scattering on two cylindrical solenoids with opposite magnetic fluxes. Complications arising in interpreting the observable cross sections are discussed and practical recommendations on the performance of the experiment are given.

As far as we know, the present calculations are the first realistic ones which treat the AB effect quantitatively, thus permitting a direct comparison with experimental data. The wavefunctions used are always single-valued both in the presence or absence of the magnetic field, in simple or multiconnected regions.

2. Scattering in the absence of the magnetic field

Consider the impenetrable cylinder of the radius R with its axis coinciding with the Z axis. For the scattering wavefunction (the initial wavevector is along the x axis) one has the following familiar equations:

$$\psi_0 = \exp(ikx) + \psi_s^0$$
$$\psi_s^0 = -2 \sum_{m=0}^{\infty} \varepsilon_m i^m H_m^{(1)}(k\rho) \frac{J_m(kR)}{H_m^{(1)}(kR)} \cos m\varphi. \tag{2.1}$$

Here $\varepsilon_m = (1+\delta_{m,0})^{-1}$; ρ and φ are the usual polar coordinates ($x = \rho\cos\varphi, y = \rho\sin\varphi$); J_m and $H_m^{(1)}$ are Bessel and Hankel functions.

From the asymptotic behaviour of ψ_s^0 ($\sim(1/\sqrt{\rho})f_0(\varphi)$) we find the scattering amplitude:

$$f_0(\varphi) = -2\left(\frac{2}{\pi i k}\right)^{1/2} \sum_m \varepsilon_m \frac{J_m(kR)}{H_m^{(1)}(kR)} \cos m\varphi. \tag{2.2}$$

For $kR \ll 1$, equations (2.1) and (2.2) transform into

$$\begin{aligned} \psi_s^0 &\approx H_0^{(1)}(k\rho)\left[1+\frac{2i}{\pi}\ln\left(\frac{kR}{2}+C\right)\right]^{-1} \\ f_0(\varphi) &\approx -\left(\frac{2}{\pi i k}\right)^{1/2}\left[1+\frac{2i}{\pi}\ln\left(\frac{kR}{2}+C\right)\right]^{-1} \end{aligned} \tag{2.3}$$

(C is Euler's constant $\approx 0.577\ldots$). For high energies the sums (2.1) and (2.2) contain many oscillating terms. In this case the Kirchoff approximation [16] turns out to be appropriate. Using it we obtain

$$\psi_s^0 = -\frac{1}{4}\int_{-R}^{R} dy' \left[H_0^{(1)}(kt) + \frac{ix}{t} H_1^{(1)}(kt)\right] \qquad (t = \sqrt{x^2+(y'-y)^2}). \tag{2.4}$$

For large values of $k\rho$

$$\psi_s^0 = -\left(\frac{2}{\pi i k}\right)^{1/2} \frac{k}{4}\int_{-R}^{R} dy' \frac{\exp(ikt)}{\sqrt{t}}\left(1+\frac{x}{t}\right). \tag{2.5}$$

With ρ and R fixed, the integrand in (2.5) oscillates rapidly as $k \to \infty$. For $|y| < R$ the main contribution to the integral is due to the stationary point ($y' = y$). The use of the stationary phase method gives

$$\psi_s^0 \approx -\exp(ikx) \qquad k \to \infty, |y| < R, x > 0. \tag{2.6}$$

Substituting this into (2.1) we get $\psi_0 \approx 0$, which corresponds to the geometrical shadow behind the cylinder. For $\rho \gg R$ it follows from (2.5) that

$$\psi_s^0 \approx -\frac{k}{4}\left(\frac{2}{\pi i k\rho}\right)^{1/2}(1+\cos\varphi)\int_{-R}^{R} \exp(ikt)\, dy'. \tag{2.7}$$

If ρ is so large that not only $k\rho \gg 1$ and $\rho \gg R$ but also $kR^2/\rho \ll 1$ (Fraunhöfer diffraction), then ψ_s^0 could be presented as a product of the outgoing wave and the scattering amplitude (which is a function of the angle solely)

$$\begin{aligned} &\psi_s^0 \approx \frac{\exp(ik\rho)}{\sqrt{\rho}} f_0(\varphi) \qquad f_0(\varphi) = -\frac{1}{\sqrt{2\pi i k}} \frac{\sin(kR\sin\rho)}{\sin\varphi}(1+\cos\varphi) \\ &\sigma_0(\varphi) = |f_0(\varphi)|^2 = \frac{1}{2\pi k}\left[\frac{1+\cos\varphi}{\sin\varphi}\sin(kR\sin\varphi)\right]^2. \end{aligned} \tag{2.8}$$

In the same way one obtains the scattering cross sections for two impenetrable cyclinders of radius R (with their axis passing through point $\pm d$ of the y axis and the initial wavevector along the x axis (see figure 1)):

$$\sigma_0^{2c} = \frac{2}{\pi k}\left[\frac{1+\cos\varphi}{\sin\varphi}\sin(kR\sin\varphi)\cos(kd\sin\varphi)\right]^2 \tag{2.9}$$

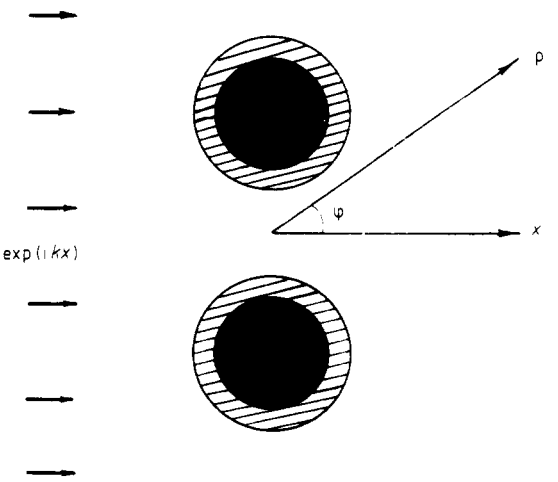

Figure 1. Electron scattering on two cylindrical solenoids with $\phi_1 = -\phi_2$ (dark circles) embedded into the impenetrable cylinders (hatched circles). The arrows show the direction of the initial wavevector. φ is the scattering angle, $\rho = \sqrt{x^2 + y^2}$.

and for the impenetrable torus (the initial wavevector along the z axis (see figure 2)):

$$\sigma_c^{\mathrm{T}} = \frac{1}{4}\left(\frac{1+\cos\theta}{\sin\theta}\right)^2 \{(d+R)J_1[k(d+R)\sin\theta] - (d-R)J_1[k(d-R)\sin\theta]\}^2. \tag{2.10}$$

The Kirchoff method works well if the ratio r of the scatterer dimension to the wavelength is much larger than 1 [16]. The fields obtained by this method differ from the exact ones only in the closest vicinity of the scatterer. The numerical investigation [17] shows that the Kirchoff method has a much broader range of applicability: it works if the above ratio only slightly exceeds unity ($r \geqslant 2$–3). In typical experiments with a single cylinder [6] one has: E (electron energy) = 20 keV and $R = 10^{-4}$ cm. This gives $kR \approx 10^6$. The same situation holds for the experiments of Tonomura *et al* [11] with the toroidal solenoid. These estimates show that the Kirchoff method is suitable for the description of the experiments under consideration.

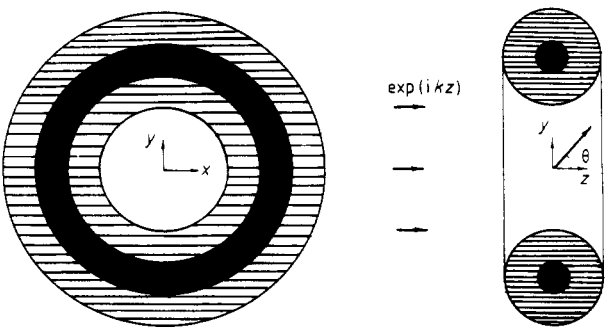

Figure 2. The electron scattering on the toroidal solenoid (darkened) surrounded by the impenetrable torus (hatched); θ is the scattering angle.

3. Scattering in the presence of the magnetic field

3.1. Single cylindrical solenoid

Let the solenoids which produce the magnetic flux ϕ be installed inside the cylinders and torus treated in the previous section. Consider first the usual single-solenoid case. The wavefunction describing the particle scattering is

$$\psi_\gamma = \psi_{AB}^\gamma + \psi_s^\gamma \qquad \gamma \equiv e\phi/hc. \tag{3.1}$$

Here ψ_{AB}^γ describes the scattering on the point non-screened solenoid [9]:

$$\psi_{AB}^\gamma = \sum_{m=-\infty}^{\infty} \exp[i\pi(|m| - \tfrac{1}{2}|m-\gamma|)] J_{|m-\gamma|}(k\rho) \exp(im\varphi). \tag{3.2}$$

ψ_s^γ takes into account the shielding and finite dimensions of the solenoid

$$\psi_s^\gamma = -\sum_{m=-\infty}^{\infty} \exp[i\pi(|m| - \tfrac{1}{2}|m-\gamma|] H_{|m-\gamma|}^{(1)}(k\rho) \frac{J_{|m-\gamma|}(kR)}{H_{|m-\gamma|}^{(1)}(kR)} \exp(im\varphi). \tag{3.3}$$

The asymptotics of ψ_s^γ is trivial

$$\begin{aligned} &\psi_s^\gamma \approx \frac{\exp(ik\rho)}{\sqrt{\rho}} f_\gamma(\varphi) \\ &f_\gamma(\varphi) = \left(\frac{2}{\pi ik}\right)^{1/2} \sum_{m=-\infty}^{\infty} \frac{J_{|m-\gamma|}(kR)}{H_{|m-\gamma|}^{(1)}(kR)} \exp[im\varphi + i\pi(|m| - |m-\gamma|)]. \end{aligned} \tag{3.4}$$

The asymptotics of ψ_{AB}^γ is rather subtle. In a closed form valid for all angles it was first obtained in [18]:

$$\psi_{AB}^\gamma \approx \exp(ikx) \exp[i\gamma(\varphi - \pi)] + i \frac{\sin \pi\gamma \exp(i\varphi/2) \exp(ik\rho)}{(1 - 2\pi\, ik\rho \sin^2(\varphi/2))^{1/2}}. \tag{3.5}$$

The case $\gamma = \frac{1}{2}$ is of particular interest:

$$\begin{aligned} &\psi_{1/2} = \psi_{AB}^{1/2} + \psi_s^{1/2} \\ &\psi_{AB}^{1/2} = -2 \exp\left(\frac{i\varphi}{2} + \frac{i\pi}{4}\right) \sum_{m=0}^{\infty} i^m J_{m+1/2}(k\rho) \sin(m + \tfrac{1}{2})\varphi \\ &\psi_s^{1/2} = 2 \exp\left(\frac{i\varphi}{2} + \frac{i\pi}{4}\right) \sum_{m=0}^{\infty} i^m H_{m+1/2}^{(1)}(k\rho) \frac{J_{m+1/2}(kR)}{H_{m+1/2}^{(1)}(kR)} \sin(m + \tfrac{1}{2})\varphi \\ &f_{1/2}(\varphi) = 2\left(\frac{2}{\pi ik}\right)^{1/2} \exp\left(\frac{i\varphi}{2}\right) \sum_{m=0}^{\infty} \frac{J_{m+1/2}(kR)}{H_{m+1/2}^{(1)}(kR)} \sin(m + \tfrac{1}{2})\varphi. \end{aligned} \tag{3.6}$$

It follows from (3.6) that $\psi_{1/2} = \psi_{AB}^{1/2} = \psi_s^{1/2} = f_{1/2} = 0$ on the positive semi-axis x ($\varphi = 0$). For $\gamma = \frac{1}{2}$ and small values of kR

$$\begin{aligned} &\psi_s^{1/2} = -2 \exp\left[i\left(\frac{\varphi}{2} - \frac{\pi}{4}\right)\right] kR H_{1/2}^{(1)}(k\rho) \sin\frac{\varphi}{2} \\ &f_{1/2} = 2\left(\frac{2}{\pi k}\right)^{1/2} \exp\left[i\left(\frac{\varphi}{2} + \frac{\pi}{4}\right)\right] kR \sin\frac{\varphi}{2}. \end{aligned} \tag{3.7}$$

3.2. The unusual direction of the initial wavevector

Let ψ_0^W be a wavefunction corresponding to scattering on an impenetrable cylinder of radius R with zero magnetic flux inside it and an impenetrable wall extending from $x = R$ to $x = \infty$ (incoming particles move along the negative x semi-axis towards the origin (see figure 3)). Then, we have the following relation [15]:

$$\psi_{1/2} = \exp\left(\frac{i\varphi}{2}\right)\psi_0^W. \tag{3.8}$$

This means that for $\gamma = \frac{1}{2}$ the presence of the magnetic flux inside the solenoid is equivalent (up to a phase factor) to the introduction of the impenetrable well. Equations similar to (3.8) are valid also for two solenoids with $\phi_1 = -\phi_2$ and for the toroidal solenoid. For the initial wavevector directed along the x axis the impenetrable wall coincides with the part of the $Y = 0$ plane lying between two solenoids (figure 4) and with the part of the $Z = 0$ plane coinciding with the torus hole (figure 5). For an infinitely thin non-shielded solenoid the relations similar to (3.8) have been obtained in [9, 19, 20]. It follows from (3.8) that for $\gamma = \frac{1}{2}$ the wavefunctions (as well as probability and current densities) vanish in places where those impenetrable walls are situated for $\gamma = 0$ (and which in fact are absent for $\gamma = \frac{1}{2}$). This means that the counting rate of particle detectors installed there (D in figure 3, D_1 in figures 4 and 5) drops to zero for $\gamma = \frac{1}{2}$. On the other hand, the counting rate of the detectors D_2 installed on the x axis after two solenoids with $\phi_1 = -\phi_2$ (figure 4) and after the toridal solenoid (figure 5) is practically the same for $\gamma = 0$ and $\gamma = \frac{1}{2}$. This is essentially the idea of the experiment proposed in [15] for testing the AB effect. It is remarkable that the sole existence of the magnetic flux in the inaccessible region pushes out the probability and current densities from the available space regions.

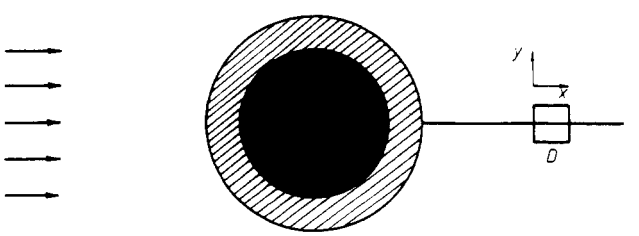

Figure 3. The cylindrical solenoid (dark circle) is embedded into the impenetrable cylinder (hatched one). For the incoming wavevector along the x axis and $\gamma = e\phi/hc = \frac{1}{2}$ the wavefunction vanishes on the x axis behind the solenoid.

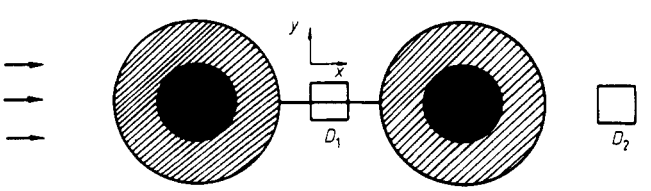

Figure 4. Two cylindrical solenoids with $\phi_1 = -\phi_2 = \phi$ (dark circles) are surrounded by the impenetrable cylinders (hatched ones). The incoming wavevector is along the x axis. For $\gamma = e\phi/hc = \frac{1}{2}$ the wavefunction vanishes on the part of the axis lying between the two cylinders.

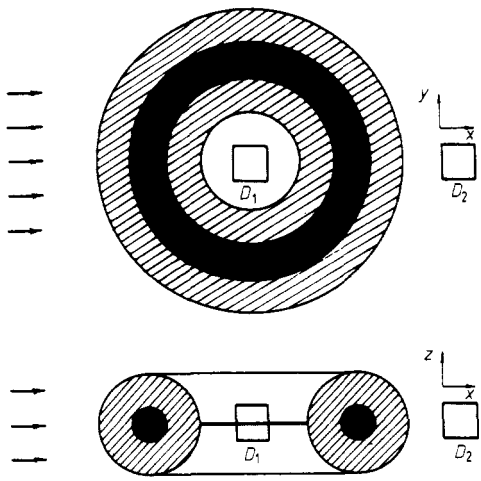

Figure 5. The toroidal solenoid (black) is embedded into the impenetrable torus (hatched). For the initial wavevector along the x axis and $\gamma = \frac{1}{2}$, the wavefunction disappears on the part of the $z = 0$ plane coinciding with the torus hole.

3.3. Two cylindrical solenoids and the toroidal solenoid

For two cylindrical solenoids with $\phi_1 = -\phi_2 = \phi$ (figure 1) the magnetic scattering amplitude equals [21]

$$f_m^B = \left(\frac{2\pi i}{k}\right)^{1/2} \gamma \frac{1+\cos\varphi}{\sin\varphi} \sin[k(d-R)\sin\varphi] \tag{3.9}$$

in the first Born approximation,

$$f_m^{HE} = -\left(\frac{2}{\pi i k}\right)^{1/2} [1-\exp(2i\pi\gamma)] \frac{\sin[k(d-R)\sin\varphi]}{\sin\varphi} \tag{3.10}$$

in the high-energy approximation and

$$f_m^D = -\frac{1}{\sqrt{2\pi i k}} [1-\exp(2i\pi\gamma)] \frac{1+\cos\varphi}{\sin\varphi} \sin[k(d-R)\sin\varphi] \tag{3.11}$$

in the Dirac phase factor approximation [22].

For the toroidal solenoid (figure 2) the corresponding magnetic amplitudes are [14]

$$f_m^B = \pi\gamma(d-R) \frac{1+\cos\theta}{\sin\theta} J_1[k(d-R)\sin\theta] \tag{3.12}$$

$$f_m^{HE} = ik(d-R)[1-\exp(2i\pi\gamma)] \frac{J_1[q(d-R)]}{q} \qquad q = 2k\sin\theta/2 \tag{3.13}$$

$$f_m^D = \frac{i}{2}[1-\exp(2i\pi\gamma)](d-R) \frac{1+\cos\theta}{\sin\theta} J_1[k(d-R)\sin\theta]. \tag{3.14}$$

For the infinitely thin toroidal solenoids the amplitudes (3.12) and (3.13) have been obtained in [13].

The conditions for the validity of these equations are well known. The first Born approximation works if the magnetic flux inside the solenoids is sufficiently small

(exactly, $\gamma \ll 1$). The high-energy approximation holds if the following conditions are satisfied (see, e.g., [23]). First, the kinetic energy of the scattered particle should considerably exceed the potential one. In the problem treated this means

$$\frac{\hbar^2 k^2}{2m} \gg \frac{\hbar^2}{2m} \frac{2ek}{\hbar c} |A_z|.$$

Here, m and k are the mass of the scattered particle and its wavenumber, A_z is the z component of the vector potential. Taking for $|A_z|$ its maximal value ($\simeq \phi/2\pi R$, see [24]) we obtain $kR \gg 2\gamma$. In the experiments of Tonomura *et al* $kR \approx 2 \times 10^6$ and $\gamma \approx 5$. So the first condition for the validity of the high-energy approximation is satisfied. The second condition for its validity is as follows: $|z| \ll k\langle r \rangle^2$. Here, z is the distance from the scatterer in the z direction (coinciding with the direction of the wavevector); $\langle r \rangle$ is the average dimension of the region inside which the potential energy essentially differs from zero. If $\langle r \rangle$ and k are equal to the parameter d ($\approx 4\,10^{-4}$ cm) of the Tonomura solenoids ($(\rho - d)^2 + z^2 = R^2$) and to the wavenumber used in the discussed experiments ($\approx 2 \times 10^{10}\,\mathrm{cm}^{-1}$), then $|z| \ll 32$ m. So the second condition is also satisfied. The validity range of the Dirac phase factor approximation is somewhat uncertain. According to Berry [22] it holds 'if in a particular angular region only two whirling waves are appreciable'. We observe that this approximation is a suitable interpolation between the 1st Born and high-energy approximations (it coincides with the former for small values of γ and with the latter for small scattering angles). For this reason and for definiteness in the following we shall use the magnetic amplitudes $f_{\mathrm{m}}^{\mathrm{D}}$.

3.4. Total scattering amplitudes and cross sections

The total scattering amplitude on the solenoid surrounded by an impenetrable barrier consists of the scattering amplitude f_0 in the absence of the magnetic field (see section 2) and of the magnetic scattering amplitude f_{m}. As a result, the following expressions are obtained for the total scattering amplitudes and cross sections

$$f_\gamma^{2\mathrm{C}} = -\frac{1}{\sqrt{2\pi i k}} \frac{1+\cos\varphi}{\sin\varphi} \{\sin[k(d+R)\sin\varphi] - \exp(2i\pi\gamma)\sin[k(d-R)\sin\varphi]\} \tag{3.15}$$

$$\sigma_\gamma^{2\mathrm{C}} = \frac{2}{\pi k}\left(\frac{1+\cos\varphi}{\sin\varphi}\right)^2 [\sin^2(kd\sin\varphi)\cos^2(kR\sin\varphi)\sin^2\pi\gamma + \sin^2(kR\sin\varphi)\cos^2(kd\sin\varphi)\cos^2\pi\gamma] \tag{3.16}$$

for two cylindrical solenoids ($\phi_1 = -\phi_2 = \phi$) and

$$f_\gamma^{\mathrm{T}} = \frac{i}{2}\frac{1+\cos\theta}{\sin\theta}\{(d+R)J_1[k(d+R)\sin\theta] - \exp(2i\pi\gamma)(d-R)J_1[k(d-R)\sin\theta]\} \tag{3.17}$$

$$\sigma_\gamma^{\mathrm{T}} = \sigma_0^{\mathrm{T}} + \left(\frac{1+\cos\theta}{\sin\theta}\right)^2 (d^2 - R^2)\sin^2\pi\gamma \times J_1[k(d+R)\sin\theta]J_1[k(d-R)\sin\theta] \tag{3.18}$$

for the toroidal solenoid. Here σ_0^T is defined by (2.10). The case $\gamma = \frac{1}{2}$ is particularly interesting:

$$\sigma_{1/2}^{2C} = \frac{2}{\pi k}\left[\frac{1+\cos\varphi}{\sin\varphi}\sin(kd\sin\varphi)\cos(kR\sin\varphi)\right]^2 \tag{3.19}$$

$$\sigma_{1/2}^{T} = \frac{1}{4}\left(\frac{1+\cos\theta}{\sin\theta}\right)^2\{(d+R)J_1[k(d+R)\sin\theta] + (d-R)J_1[k(d-R)\sin\theta]\}^2. \tag{3.20}$$

4. The experimental consequences

4.1. One cylindrical solenoid

Now we discuss the observable consequences of the considerations developed in the last two sections. At first, we elucidate the conditions for which the gedanken experiment mentioned in section 3.2 could be realised. We take one cylindrical solenoid as an example. Comparing (2.3) with (3.7) we note that a maximal distinction of the wavefunctions for $\gamma = 0$ and $\gamma = \frac{1}{2}$ takes place for small kR. For finite values of kR and $k\rho \to \infty$ the cross section oscillates with period π/kR (see (2.8)). The oscillation amplitude is particularly large for small angles. The introduction of the impenetrable wall (this is equivalent to switching on the magnetic flux inside the solenoid with $\gamma = \frac{1}{2}$) changes the diffraction pattern. But an essential decreasing of the wavefunction takes place in the nearest vicinity of the positive x semiaxis. Now we evaluate $|\psi|^2$ behind the solenoid for the intermediate values of kR and $k\rho$. For this we compute the wavefunction defined by (2.1) and (3.6). In figures 6 and 7 we present numerical results for $kR = 1$ and $kR = 10$ for different values of $k\rho$. For convenicnce, $|\psi_{1/2}(\rho, \varphi)|^2$

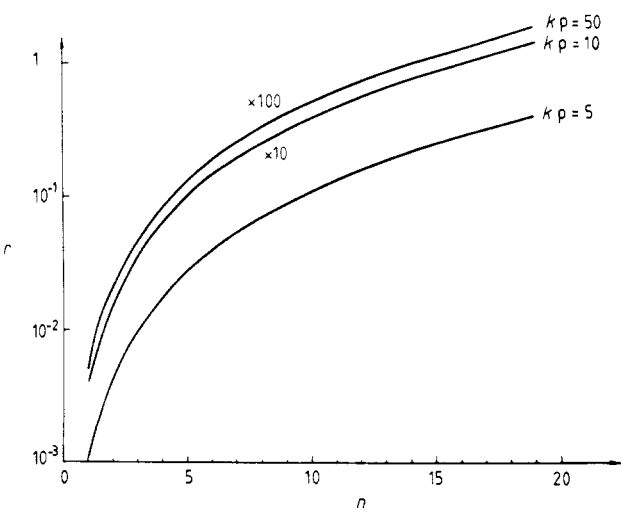

Figure 6. Illustration of the magnetic field influence on the particle probability in the shadow region. On the vertical axis the ratio $r = |\psi_{1/2}(\rho, \varphi)/\psi_0(\rho, \varphi = 0)|^2$ is presented. φ is expressed through the number n (presented on the horizontal axis) as follows: $\varphi = [(n-1)/21]\sin^{-1}R/\rho$. The value of $kR = 1$.

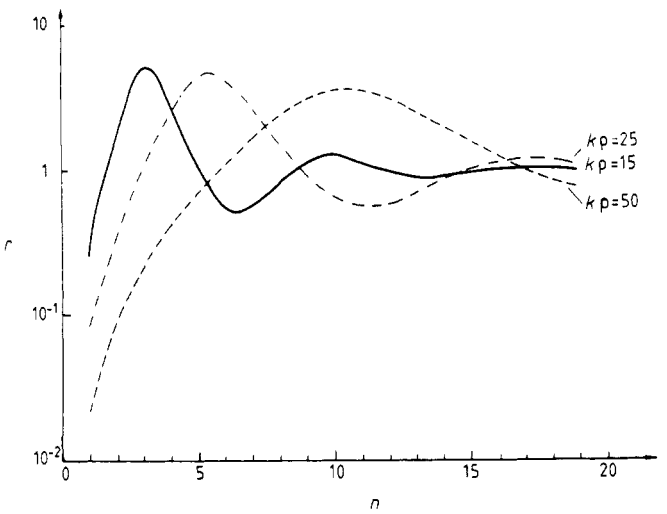

Figure 7. The same as in figure 6 but for $kR = 10$.

is related to the absolute square of the wavefunction in the absence of the magnetic field taken on the x axis for the same value of ρ. Thus, on the vertical axis the ratio $r = |\psi_{1/2}(\rho, \varphi)/\psi_0(\rho, \varphi = 0)|^2$ is presented. On the horizontal axis, the number n is given, to which the angle $\varphi = ((n-1)/21)\sin^{-1} R/\rho$ $(n = 1, \ldots, 21)$ corresponds. (For definiteness the shadow region $(0 \leqslant |\varphi| \leqslant \sin^{-1} R/\rho)$ was divided into 40 equal parts. As absolute values of the wavefunction for $\gamma = 0$ and $\gamma = \frac{1}{2}$ are even functions of φ, it is enough to evaluate $|\psi|^2$ only for positive angles.) From figures 6 and 7 we see that an increasing wavenumber leads to the appearance of oscillations and to the narrowing of the region with small $|\psi_{1/2}|^2$. For very large values of kR and $k\rho$ occurring in experiments [6] the region behind the solenoid is in shadow. The wavefunction is extremely small there. The introduction of the impenetrable wall extending from $x = R$ to $x = \infty$ (this is equivalent to the creation of the magnetic flux with $\gamma = \frac{1}{2}$ inside the solenoid) does not change anything. At first glance it seems that in these circumstances the realisation of the experiments mentioned in section 3.2 is useless. This is not the case. The reason is that in these experiments negatively charged electrostatic systems (so-called biprisms) are used, deflecting electrons towards the x axis. Effectively this is equivalent to reduction of the wavenumber. As a result the diffraction pattern reappears in the shadow region. If biprisms are situated symmetrically relative to the x axis and carry the same negative potential, the wavefunction for $\gamma = \frac{1}{2}$ vanishes as before on the x axis. This could be verified experimentally.

4.2. Two impenetrable solenoids

Now we discuss the experimental consequences of the electron scattering on two impenetrable solenoids with $\phi_1 = -\phi_2$ (figure 1). It follows from (2.9) that in the absence of the magnetic field the scattering cross section has two families of zeros at angles defined by

$$\sin \varphi_n^{(R)} = \frac{n\pi}{kR} \qquad \sin \varphi_n^{(d)} = \frac{n - \frac{1}{2}}{kd}\,\pi \tag{4.1}$$

or, if n is not too large,

$$\varphi_n^{(R)} \approx \frac{n\pi}{kR} \qquad \varphi_n^{(d)} \approx \frac{n-\frac{1}{2}}{kd}\pi. \tag{4.2}$$

On the other hand, for $\gamma = \frac{1}{2}$

$$\varphi_n^{(R)} \approx \frac{n+\frac{1}{2}}{kR}\pi \qquad \varphi_n^{(d)} \approx \frac{n\pi}{kd}. \tag{4.3}$$

Comparing (4.2) with (4.3) we conclude that the magnetic field shifts zeros of the cross section on $\pi/2kR$ (for the first family) and on $\pi/2kd$ (for the second family). In the experiments one does not see zeros of the cross section but its maxima. In figure 8 we present the cross sections evaluated for the following parameter: $k = 2\times10^{10}\,\mathrm{cm}^{-1}$, $R = 10^{-4}$ cm, $d = 5\times10^{-4}$ cm. On the horizontal axis the scattering angle is presented. The origin corresponds to the angle $\varphi = 0.01°$. The numbers on this axis correspond to the excess over 0.01° in units of 10^{-5} deg. For example, number 5 corresponds to the angle $(10^{-2}+5\times10^{-5})°$. The cross sections given by (3.16) are presented on the vertical axis. The full, broken and dotted curves correspond to $\gamma = 0$, 0.5 and 0.25, respectively. We observe that positions of maxima are rather irregular. For instance, the maximum of $\sigma_{1/2}^{2c}$ does not always occur between two successive maxima of σ_0^{2c}. To clarify this we present in the upper part of figure 9 the positions and magnitudes of maxima both for $\gamma = 0$ and $\gamma = \frac{1}{2}$.

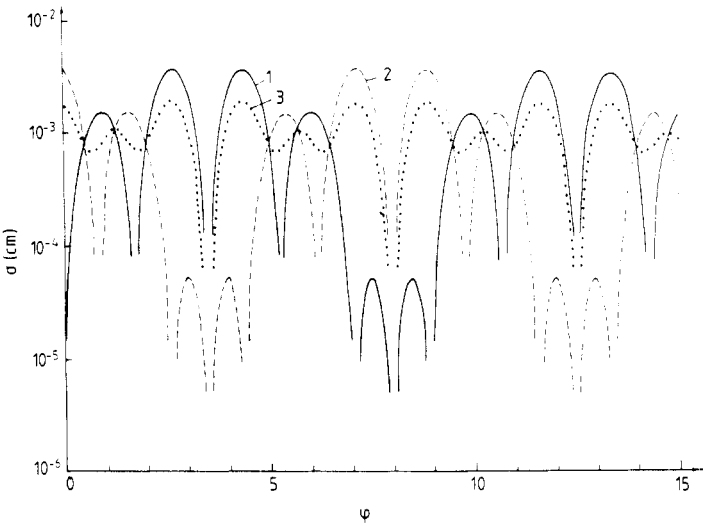

Figure 8. The electron cross section on two solenoids with $\phi_1 = -\phi_2$. On the horizontal axis the origin corresponds to $\varphi = 0.01°$. The numbers on it are the excess over 0.01° in units of 10^{-5} deg. For example, number 5 corresponds to the angle $(0.01\times5\times10^{-5})°$. In Fraunhöfer diffraction theory curves 1, 2 and 3 correspond to $\gamma = 0$, 0.5 and 0.25. The situation changes drastically if one uses Fresnel diffraction theory. If ρ (distance from the origin to the point of measurement (see figure 1)) equals 106.1 cm, then Fresnel theory exactly reproduces the Fraunhöfer cross sections with the same values of γ. If $\rho = 91$ cm, then curves 1, 2 and 3 correspond to $\gamma = 0.5$, 0 and 0.25. For $\rho \approx 98$ cm the cases $\gamma = 0$ and $\gamma = 0.5$ are described by the same curve 3.

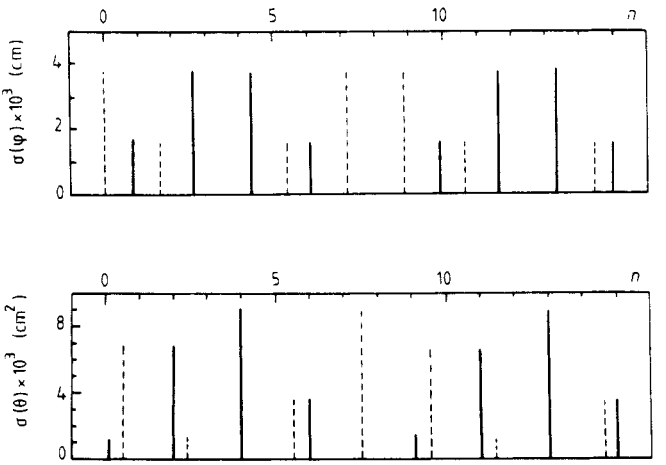

Figure 9. The positions and values of the cross section maxima for two cylinders with $\phi_1 = -\phi_2$ (upper part) and for the toroidal solenoid (the lower one). The full vertical lines correspond to $\gamma = 0$, the broken ones to $\gamma = 0.5$.

4.3. The toroidal solenoid

Now we consider the electron scattering on the toroidal solenoid. Because for real experiments (which will be discussed below) $kd \gg 1$ and $kR \gg 1$ in (2.10), (3.18) and (3.20) for angles not too small one may, instead of the Bessel functions, use their asymptotic values:

$$\sigma_0^{\mathrm{T}} \approx \frac{1}{2\pi k} \frac{(1+\cos\theta)^2}{\sin^3\theta} \{\sqrt{d+R}\sin[k(d+R)\sin\theta - (\pi/4)] - \sqrt{d-R}\sin[k(d-R)\sin\theta - (\pi/4)\}^2 \tag{4.4}$$

$$\sigma_{1/2}^{\mathrm{T}} \approx \frac{1}{2\pi k} \frac{(1+\cos\theta)^2}{\sin^3\theta} \{\sqrt{d+R}\sin[k(d+R)\sin\theta - (\pi/4)]\sqrt{d-R}\sin[k(d-R)\sin\theta - (\pi/4)]\}^2. \tag{4.5}$$

If, in addition, $R \ll d$ then one may disregard R under the square root but not inside sin or cos (as $kR \gg 1$):

$$\sigma_0^{\mathrm{T}} = \frac{2d}{\pi k} \frac{1}{\sin^3\theta} [(1+\cos\theta)\sin(kR\sin\theta)\cos(kd\sin\theta - (\pi/4)]^2 \tag{4.6}$$

$$\sigma_{1/2}^{\mathrm{T}} = \frac{2d}{\pi k} \frac{1}{\sin^3\theta} [(1+\cos\theta)\cos(kR\sin\theta)\sin(kd\sin\theta - (\pi/4)]^2. \tag{4.7}$$

Just as for two cylinders, one has two families of zeros:

$$\theta_n^{(R)} \approx \frac{n\pi}{kR} \qquad \theta_n^{(d)} \approx \frac{n-\frac{1}{4}}{kd}\pi \qquad \text{for } \gamma = 0 \tag{4.8}$$

$$\theta_n^{(R)} z \frac{n+\frac{1}{2}}{kR}\pi \qquad \theta_n^{(d)} \approx \frac{n+\frac{1}{4}}{kd}\pi \qquad \text{for } \gamma = \tfrac{1}{2}. \tag{4.9}$$

When the magnetic field is switched on, the zeros of the first and second families shift on $\Delta\theta_R \approx \pi/2kR$ and $\Delta\theta_d \approx \pi/2kd$, respectively. The excellent experiments of Tonomura *et al* [11] were performed with the following parameters: E (electron energy) = 150 keV, $R = 10^{-4}$ cm, $d = 4\times10^{-4}$ cm. Then $k = 2\times10^{10}\text{cm}^{-1}$, $kR = 2\times10^{6}$, $kd = 8\times10^{6}$. This gives $\Delta\theta_R \approx 8\times10^{-7}$ and $\Delta\theta_d \approx 2\times10^{-7}$. The shift of the diffraction maxima was observed in the plane normal to the wavevector of the incoming wave (i.e. in the plane z = constant, figure 2). Unfortunately the authors [11] did not indicate the distance from the toroidal solenoid to the plane where the diffraction pattern was observed. From the drawing of the installation presented in [11] we estimate this distance to be equal approximately to 1 m. Then for the shift of zeros one obtains $\Delta z_R \approx r\Delta\theta_R \approx 0.8\ \mu$m, $\Delta z_d \approx r\Delta\theta_d \approx 0.2\ \mu$m. Shifts of the same order were observed in [11]. The typical angular dependence of the cross sections defined by (2.10) and (3.20) is shown in figure 10. The positions and values of maxima are shown in the lower part of figure 9.

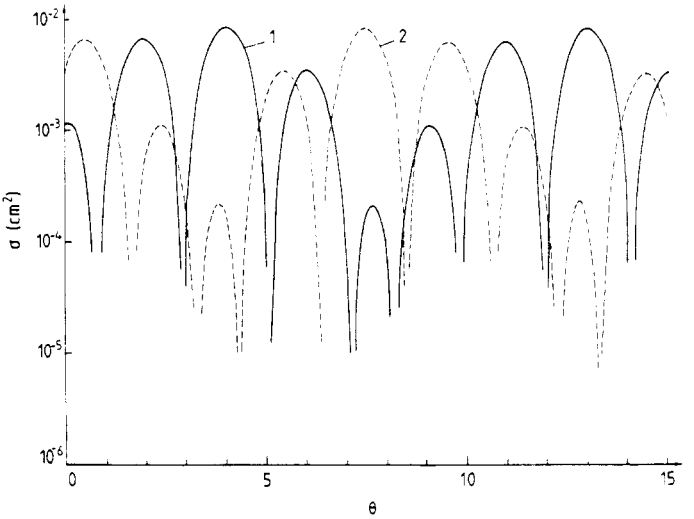

Figure 10. The electron cross sections on the toroidal solenoid. The cases $\gamma = 0$ and $\gamma = 0.5$ are shown by the full and broken curves, respectively.

4.4. Scattering cross sections

The presentation of the scattered wave as a product of the outgoing wave ($=\exp(ik\rho)/\sqrt{\rho}$ for the two-dimensional case and $\exp(ikr)/r$ for the three-dimensional one) and the term depending only on angles is valid for sufficiently large distances from the scatterer. In addition to the conditions $kr \gg 1$ and $R/r \ll 1$ (which we always assume to be satisfied), the relation $kR^2/r \ll \pi$ should be fulfilled for the scattering on single cylinder, and the relation $kdR/r \ll \pi$ for scattering on two cylinders and on the torus. In optics the scattering under these conditions is called Fraunhöfer diffraction. In the experiments performed with single solenoid [6] one has $kR^2/r \approx 5$. In the experiments of Tonomura *et al* $kdR/r \approx 8$ (if r is chosen to be equal to 1 m). As the conditions for the validity of the Fraunhöfer diffraction are violated, the results of sections 4.2 and 4.3 are of a qualitative nature. To obtain quantitative results we should retain

under the exponential in (2.7) the quadratic terms and disregard the cubic ones which are small (in fact, for one cylinder $kR^2/\rho^2 \approx 3\times 10^{-5}$; for the torus $kdR^2/r^2 \approx 8\times 10^{-6}$). In optical language this is called Fresnel diffraction. We illustrate how the previous results are changed using electron scattering on two cylindrical solenoids with $\phi_1 = -\phi_2$ as an example. If the above conditions ($kd \gg 1$, $\rho \gg d$, $kdR^2/\rho^2 \ll 1$) are satisfied, then the wavefunction equals

$$\psi = \exp(ikx) + \psi_S \tag{4.10}$$

$$\psi_s = -\frac{1}{2\sqrt{2i}}\frac{1+\cos\varphi}{\cos\varphi}\exp[ik\rho(1-\tfrac{1}{2}\tan^2\varphi)](A+iB). \tag{4.11}$$

Here we put

$$A = C_1 + C_3 - \cos 2\pi\gamma(C_2+C_4) + \sin 2\pi\gamma(S_2+S_4)$$

$$B = S_1 + S_3 - \cos 2\pi\gamma(S_2+S_4) - \sin 2\pi\gamma(C_2+C_4)$$

$$C_i = C(\rho_i) \qquad S_i = S(\rho_i) \qquad i = 1,\ldots,4$$

$$\rho_1 = \left(\frac{K\rho}{\pi}\right)^{1/2}\left(\frac{d+R}{\rho}\cos\varphi + \tan\varphi\right) \qquad \rho_2 = \left(\frac{K\rho}{\pi}\right)^{1/2}\left(\frac{d-R}{\rho}\cos\varphi + \tan\varphi\right)$$

$$\rho_3 = \left(\frac{K\rho}{\pi}\right)^{1/2}\left(\frac{d+R}{\rho}\cos\varphi - \tan\varphi\right) \qquad \rho_4 = \left(\frac{K\rho}{\pi}\right)^{1/2}\left(\frac{d-R}{\rho}\cos\varphi - \tan\varphi\right).$$

$C(x)$ and $S(x)$ are the usual Fresnel integrals

$$C(x) = \int_0^x \cos\left(\frac{\pi x^2}{2}\right)dx \qquad S(x) = \int_0^x \sin\left(\frac{\pi x^2}{2}\right)dx.$$

For $|\tan\varphi| \gg (d+R)/\rho$, equation (4.11) is simplified:

$$\psi_S = \frac{\exp(ik\rho)}{\sqrt{\rho}} f_\gamma(\rho,\varphi)$$

$$f_\gamma(\rho,\varphi) = -\frac{1}{\sqrt{2\pi ik}}\frac{1+\cos\varphi}{\sin\varphi}\left[\exp\left(ik\frac{(d+R)^2}{2\rho}\cos^2\varphi\right)\sin[k(d+R)\sin\varphi]\right.$$
$$\left. - \exp(2i\pi\gamma)\exp\left(ik\frac{(d-R)^2}{2\rho}\cos^2\varphi\right)\sin[k(d-R)\sin\varphi]\right]. \tag{4.12}$$

If the measuring device is outside the incoming electron beam (D_1, figure 11), then $|f_\gamma|^2$ coincides up to terms of the order $[(d+R)/\rho]^2$ with the particle flux through the cylindrical surface of the radius ρ and may be viewed as an analogue of the scattering cross section for the finite distances from the scatterer

$$\tilde{\sigma}_\gamma^{2C}(\rho,\varphi) = \frac{2}{\pi k}\left(\frac{1+\cos\varphi}{\sin\varphi}\right)^2\left[\sin^2(kd\sin\varphi)\cos^2(kR\sin\varphi)\sin^2\left(\frac{kdR}{\rho}\cos^2\varphi - \pi\gamma\right)\right.$$
$$\left. + \sin^2(kR\sin\varphi)\cos^2(kd\sin\varphi)\cos^2\left(\frac{kdR}{\rho}\cos^2\varphi - \pi\gamma\right)\right]. \tag{4.13}$$

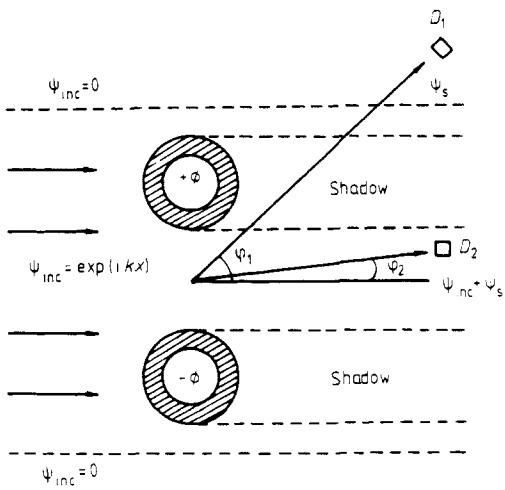

Figure 11. The detecors D_1 and D_2 in different physical conditions. Although D_2 is in the incoming beam, its position is more suitable for the detection of the diffraction pattern shift.

Obviously, $\tilde{\sigma}_\gamma^{2C}$ transforms into σ_γ^{2C} defined by (3.16) in the limit $\rho\to\infty$. The cases $\gamma=0$ and $\gamma=\frac{1}{2}$ are of particular interest

$$\tilde{\sigma}_0^{2C}=\frac{2}{\pi k}\left(\frac{1+\cos\varphi}{\sin\varphi}\right)^2\left[\sin^2(kd\sin\varphi)\cos^2(kR\sin\varphi)\sin^2\left(\frac{kdR}{\rho}\cos^2\varphi\right)\right.$$
$$\left.+\sin^2(kR\sin\varphi)\cos^2(kd\sin\varphi)\cos^2\left(\frac{kdR}{\rho}\cos^2\varphi\right)\right] \tag{4.14}$$

$$\tilde{\sigma}_{1/2}^{2C}=\frac{2}{\pi k}\left(\frac{1+\cos\varphi}{\sin\varphi}\right)^2\left[\sin^2(kd\sin\varphi)\cos^2(kR\sin\varphi)\cos^2\left(\frac{kdR}{\rho}\cos^2\varphi\right)\right.$$
$$\left.+\sin^2(kR\sin\varphi)\cos^2(kd\sin\varphi)\sin^2\left(\frac{kdR}{\rho}\cos^2\varphi\right)\right]. \tag{4.15}$$

Curious complications arise when one tries to interpret the measurements performed at finite distances from the solenoids in terms of the Fraunhöfer cross sections (2.9), (2.10), (3.19) and (3.20). We illustrate this using two solenoids with $\phi_1=-\phi_2$ as an example. Usually [6, 11] the experimenters consider a limited number of diffraction maxima and observe their shift when the magnetic field is switched on. For definiteness let the number of the observed maxima equal 10. If the parameters k, R and d are the same as in the experiments of Tonomura *et al* on the toroidal solenoid, these maxima occupy the angular range (see (4.2) and (4.3)) equal to $10\pi/kd\approx 2\times10^{-6}$. Let the measurements be performed in the neighbourhood of the angle φ_0. As $kdR/\rho\approx 8$ for $\rho=1$ m, then in (4.13)-(4.15) one may replace φ by φ_0 in $\sin((kdR/\rho)\cos^2\varphi-\pi\gamma)$ and $\cos((kdR/\rho)\cos^2\varphi-\pi\gamma)$. This substitution is invalid in $kR\sin\varphi$ and $kd\sin\varphi$ as (in view of $kR\gg1$ and $kd\gg1$) they vary considerably at

the angle interval $10\pi/kd$. Then, instead of (4.13) one has

$$\tilde{\sigma}_{\gamma}^{2C} \approx \frac{2}{\pi k}\left(\frac{1+\cos\varphi}{\sin\varphi}\right)^2 [\sin^2(kd\sin\varphi)\cos^2(kR\sin\varphi)\sin^2(\omega-\pi\gamma) + \sin^2(kR\sin\varphi)\cos^2(kd\sin\varphi)\cos^2(\omega-\pi\gamma)] \qquad \omega = \frac{kdR}{\rho}\cos^2\varphi_0. \tag{4.16}$$

Consider the particular cases ($\gamma = 0, \frac{1}{2}$) of (4.16):

$$\tilde{\sigma}_0^{2C} = \frac{2}{\pi k}\left(\frac{1+\cos\varphi}{\sin\varphi}\right)^2 [\sin^2(kd\sin\varphi)\cos^2(kR\sin\varphi)\sin^2\omega + \sin^2(kR\sin\varphi)\cos^2(kd\sin\varphi)\cos^2\omega] \tag{4.17}$$

$$\tilde{\sigma}_{1/2}^{2C} = \frac{2}{\pi k}\left(\frac{1+\cos\varphi}{\sin\varphi}\right)^2 [\sin^2(kd\sin\varphi)\cos^2(kR\sin\varphi)\cos^2\omega + \sin^2(kR\sin\varphi)\cos^2(kd\sin\varphi)\sin^2\omega]. \tag{4.18}$$

Let ω be equal to $n\pi$. Then $\tilde{\sigma}_0^{2C} = \sigma_0^{2C}$, $\tilde{\sigma}_0^{2C}$, $\tilde{\sigma}_{1/2}^{2C} = \sigma_{1/2}^{2C}$ and the formulae of the Fraunhöfer diffraction correctly described the diffraction pattern both in the presence and absence of the magnetic field. Now let $\omega = (n+\frac{1}{2})\pi$. Then, $\tilde{\sigma}_0^{2C} = \sigma_{1/2}^{2C}$, and $\tilde{\sigma}_{1/2}^{2C} = \sigma_0^{2C}$. This means that an observer having measured the cross section for $\gamma = \frac{1}{2}$ finds that it agrees perfectly with the Fraunhöfer cross section in the absence of the magnetic field. On these grounds we deny the existence of the AB effect. One may argue that a real experimenter would not use the theoretical formulae (2.9) and (3.19). He would simply measure the diffraction patterns for $\gamma = 0$ and $\gamma = \frac{1}{2}$. Their distinction he would attribute to the existence of the AB effect. But let $\rho = \rho_0$ and φ_0 in (4.17) and (4.18) be such that $\omega = (n+\frac{1}{4})\pi$. Then $\tilde{\sigma}_{1/2}^{2C} = \tilde{\sigma}_0^{2C}$. This means that measurements performed at $\rho = \rho_0$ and $\varphi = \varphi_0$ give the same diffraction pattern for $\gamma = 0$ and $\gamma = \frac{1}{2}$. To illustrate this we again turn to figure 8. We mentioned earlier that the Fraunhöfer cross sections presented there describe the experimental situation only qualitatively. Using the formulae of Fresnel diffraction theory and choosing $\rho = 106.1$ cm ($\omega \approx 3\pi$) we exactly reproduce the Fraunhöfer cross sections 1, 2 and 3 with $\gamma = 0$; 0.5 and 0.25, respectively. Let $\rho \approx 90.95$ cm ($\omega \approx 3.5\,\pi$). Then, curves 1 and 2 correspond to $\gamma = 0.5$ and $\gamma = 0$, respectively. Curve 3 corresponds to the same γ (=0.25). Finally, for $\rho = 98$ cm ($\omega = 3.25\pi$) the values of $\gamma = 0$ and $\gamma = \frac{1}{2}$ are described by the same curve 3. As a result, one should be very cautious when interpreting the results of electron scattering on solenoids. It may happen that two observers having installed their detectors at different distances from the solenoid would come to different conclusions on the existence of the AB effect (one observer would see the shift of the diffraction pattern while the other would not). For two solenoids with $\phi_1 = -\phi_2$ the second observer should shift its detector in the radial direction by the value $\Delta\rho = \rho[-1+(4kdR/\pi\rho_0)\cos^2\varphi_0]^{-1}$ in order to obtain the correct (in the sense of the intuitive Fraunhöfer theory) value of the diffraction pattern shift.

Formulae (4.12)-(4.18) are valid if the angle at which the measurement is performed is sufficiently large ($|\tan\varphi| \gg (d+R)/\rho$). For small angles ($|\tan\varphi| < (d-R)/\rho$) the detector ($D_2$, figure 11) is in the initial beam. In this situation the cross section is not equal to the absolute square of the coefficient at the outgoing wave. According to general rules of quantum mechanics [25], it is proportional to the radial component

of the probability current through the cylindrical surface of the radius ρ: $\sigma = m\rho/\hbar k j_\rho$,

$$j = \frac{\hbar}{2im}(\bar{\psi}\,\mathrm{grad}\,\psi - \psi\,\mathrm{grad}\,\bar{\psi}) - \frac{e}{mc}\boldsymbol{A}\cdot\bar{\psi}\psi. \tag{4.19}$$

Here ψ is a complete wavefunction defined by (4.10). Substituting into (4.19) and disregarding the terms of the orders d^2/ρ^2 and $d/(k\rho^3)^{1/2}$ one obtains in the angular region treated $(0 \leqslant \varphi \leqslant (d-R)/\rho)$

$$\sigma = \rho\left[\cos\varphi + \frac{1}{8}\left(\frac{1+\cos\varphi}{\cos\varphi}\right)^2(A^2+B^2) - \frac{(1+\cos\varphi)^2}{2\sqrt{2}\cos\varphi}(A\cos\Delta + B\sin\Delta)\right]$$
$$-\frac{e\rho}{\hbar ck}\left[1 + \frac{1}{8}\left(\frac{1+\cos\varphi}{\cos\varphi}\right)^2(A^2+B^2) - \frac{1+\cos\varphi}{\sqrt{2}\cos\varphi}(A\cos\Delta + B\sin\Delta)\right]. \tag{4.20}$$

Here A and B are defined in (4.11) and

$$\Delta = k\rho(\cos\varphi - 1 + \tfrac{1}{2}\tan^2\varphi) + \pi/4.$$

For small values of φ the quantity $\cos\varphi - 1 + \frac{1}{2}\tan^2\varphi$ equals $9\varphi^4/24$. Taking for φ its maximal value $(\varphi_0 = (d-R)/\rho \approx 4\times 10^{-6})$, we get $k\rho(\cos\varphi - 1 + \frac{1}{2}\tan^2\varphi) \leqslant 3\times 10^{-11}$. So we may put $\Delta \approx \pi/4$. Now estimate the contribution to the probability current from the term proportional to the vector potential. For two solenoids with $\phi_1 = -\phi_2$ with the axes passing through the points $y = \pm d$ the radial component of $\boldsymbol{A}$ equals

$$A_\rho = \frac{\phi d\cos\varphi}{\pi(d^2+\rho^2)}\left(1 - \frac{4d^2\rho^2}{(d^2+\rho^2)^2}\sin^2\varphi\right)^{-1}.$$

In the treated case $\rho \gg d$, thus $A_\rho \approx \phi d\cos\varphi/\pi\rho^2$ and

$$\frac{e\rho}{\hbar ck}A_\rho \approx \rho\gamma\frac{2d}{k\rho^2} \approx \rho\gamma\times 5\times 10^{-18}.$$

Choose for $\gamma = e\phi/hc$ the same value as in the experiments of Tonomura *et al* ($\gamma \approx 5$). Then, the contribution of the vector potential can be disregarded. As a result, σ turns out to be proportional to $|\psi|^2$:

$$\sigma = \rho|\psi|^2$$
$$|\psi|^2 = 1 + \tfrac{1}{2}(A^2+B^2) - A - B. \tag{4.21}$$

In figures 12-14 the angular dependence of $|\psi|^2$ is shown for three different distances ($\rho \approx 106.1$; 90.95; 97.94) in the interval $-\varphi_0 < \varphi < \varphi_0$, $\varphi_0 = (d-R)/\rho$. What can we learn from these figures? First, there are no indeterminacies which are due to the coincidence of the cross sections for $\gamma = 0$ and $\gamma = \frac{1}{2}$ (see section 4.5). Second, the maximal deviation of $|\psi|^2$ from its plane-wave value (equal to 1) is about 70%. The $|\psi|^2$ maxima for $\gamma = \frac{1}{2}$ are well separated from those for $\gamma = 0$ and this could be observed experimentally. The fall of $|\psi|^2$ in the right-hand sides of figures 12-14 is due to the proximity of the shadow region. In figure 15 we present the positions and values of $|\psi|^2$ maxima in the treated angular region.

In deriving (4.20) we have assumed that a detector situated in the incoming wave (D_2, figure 11) could not distinguish the scattered particles from those of the initial beam. If the detector is constructed in such a way that it registers only scattered particles (probably a sort of colimator has been provided), then one should use in (4.19) the scattered wave ψ_s (see 4.1) instead of ψ. This results in

$$\sigma = \tfrac{1}{8}\rho\left(\frac{1+\cos\varphi}{\cos\varphi}\right)^2(A^2+B^2)\left(1 - \frac{e}{\hbar ck}A_\rho\right). \tag{4.22}$$

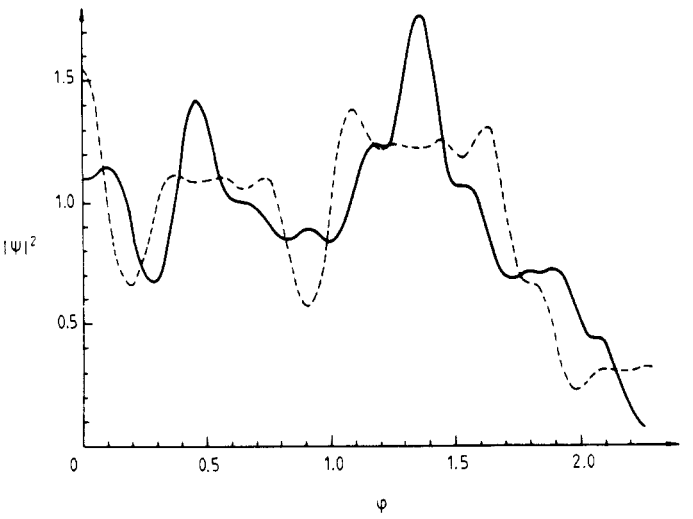

Figure 12. The probability density for electron scattering on two solenoids with $\phi_1 = -\phi_2$. The distance ρ from origin to the detector (D_2, figure 11) is taken to be 106.1 cm. The cases $\gamma = 0$ and $\gamma = 0.5$ are shown by the full and broken curves, respectively. On the horizontal axis the scattering angle (in degrees) is presented.

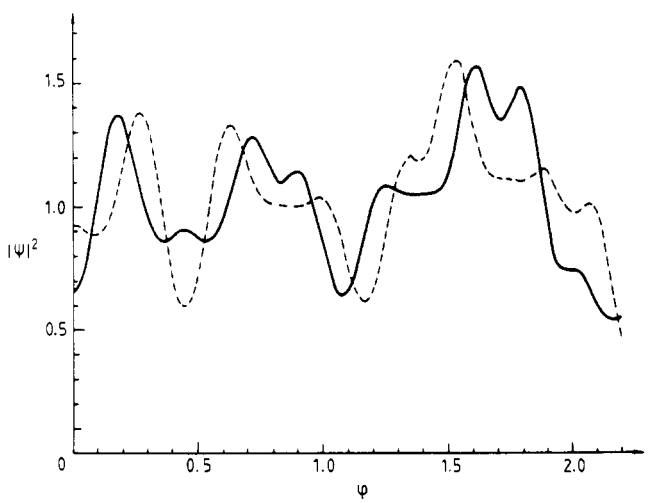

Figure 13. The same as in figure 12 but for $\rho \approx 91$ cm.

5. Discussion

We emphasise the urgent necessity of the quantitative verification of the AB effect (which sometimes is defined as observable consequences of the hidden fields). In the physical literature there exist few alternative interpretations of the observed diffraction pattern shift (see e.g. [26-29] and particularly an exciting discussion (p 307) after the Pozzi and Matteucci report (p 297) in [30]). These explanations are of the pure qualitative nature. Because of this, the experimental confirmation of the theoretically

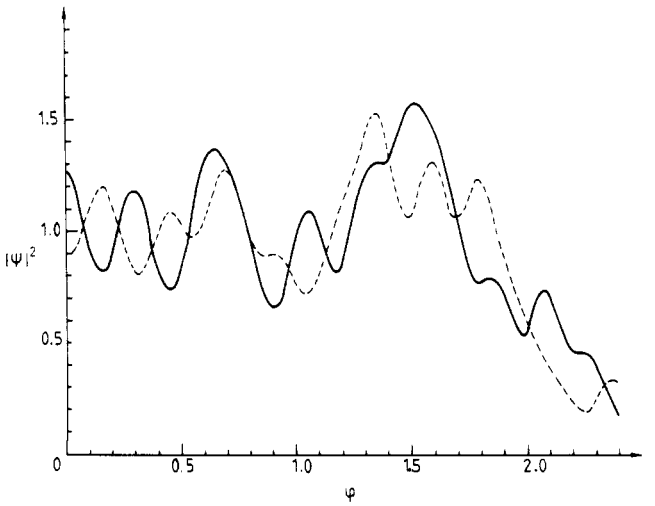

Figure 14. The same as in figure 12 but for $\rho \approx 98$ cm.

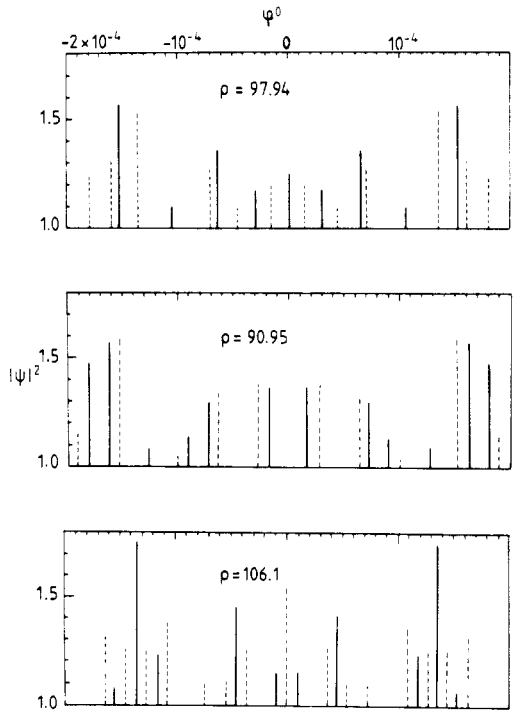

Figure 15. The positions and values of the $|\psi|^2$ maxima. The cases $\gamma = 0$ and $\gamma = 0.5$ are shown by the full vertical lines. Only those maxima are presented which exceed 1.

computed diffraction pattern shifts will be a decisive argument in favour of the physical meaning of the vector potential. It would be highly improbable if two different mechanisms give the same quantiative shift of the diffraction pattern. In our opinion the following experiments may remove doubts as to the existence of the AB effect occurring in the physical literature.

(1) Experiments with electron scattering on cylindrical and toroidal solenoids with configurations of the incident wavevector and detectors shown in figures 3-5. The Fresnel electrostatic biprisms being used, the detectors D, D_1 and D_2 should register particles in the absence of the magnetic field even for very large values of kR and kd. For $\gamma = \frac{1}{2}$ the counting rate of D and D_1 drops to zero while that of D_2 remains practically the same. Being very specific, this effect probably could not be obtained in the above mentioned alternative interpretations of the AB effect.

(2) Electron scattering on two cyclindrical solenoids with opposite magnetic fluxes for the configurations shown in figure 11. The numerical studies of section 4 show that the best place for the detector is the region of small angles. The formulae (see section 4.4) describing the cross sections quantitatively both in the presence and absence of the magnetic field show that this experiment can be realised within the existing facilities.

(3) Electron scattering on a toroidal solenoid. The Fraunhöfer diffraction theory describes these experiments only qualitatively (see section 4.4). Let us estimate at what distance from the solenoid the measuring device should be installed in order for the Fraunhöfer theory to be applicable. It works if the parameter $\omega = kdR/r \ll \pi$. If we decree ω equal to 0.1 to be small enough while for k, d and R take the same values as in the experiments of Tonomura *et al* ($k = 2 \times 10^{10}\,\mathrm{cm}^{-1}$, $R = 10^{-4}\,\mathrm{cm}$, $d = 4 \times 10^{-4}\,\mathrm{cm}$), then $r \approx 80\,\mathrm{m}$. Clearly these dimensions of the experimental installation are unacceptable. We have mentioned earlier that it is the Fresnel diffraction that describes adequately the electron scattering in the experiments of Tonomura *et al*. Unfortunately, we have not up to now succeeded in otabining the Fresnel cross sections in a closed form.

6. Conclusion

We summarise briefly the main results obtained.

(1) Using Fraunhöfer diffraction theory we investigated the electron scattering on two solenoids with opposite magnetic fluxes and on the toroidal solenoid. The diffraction patterns are obtained in both the presence and absence of the magnetic field. Explicit values are obtained for the magnetic field shift of the diffraction pattern.

(2) The experiment suggested earlier [15] testing the existence of the AB effect is investigated numerically. It is shown that it can indeed be realised within the existing experimental facilities.

(3) We demonstrate that electron scattering on two cylinders with $\phi_1 = -\phi_2$ and on the toroidal solenoid for realistic dimensions of the experimental installation is described adequately by the Fresnel diffraction theory. For two solenoids the cross sections are obtained in a closed form. The complications arising in the interpretation of the observed cross sections are discussed and the practical recommendations for the performance of experiments are given.

After submission of this paper we obtained (Afanasiev G N 1989 *JINR Preprint P4-89-357, Dubna*) the Fresnel wavefunction for the electron scattering on the toroidal

solenoid (see figure 2). It looks as follows (r and θ are the usual spherical coordinates):

$$\psi = \exp(ikz) + \psi_s$$

$$\psi_s = \frac{i}{2}(1+\cos\theta)\exp(ikz)\left[\exp\left(ik\frac{(d+R)^2}{2r}\right)W_1 - \exp(2i\pi\gamma)\exp\left(ik\frac{(d-R)^2}{2r}\right)W_2\right].$$

Functions W_1 and W_2 are expressed through the well known Lommel functions U_1 and U_2 (see any treatise on the Bessel functions)

$$W_{1,2} = U_1\left(\frac{k(d\pm R)^2}{r}, k(D\pm R)\sin\theta\right) - iU_2\left(\frac{k(d\pm R)^2}{r}, k(d\pm R)\sin\theta\right).$$

On the Z axis $|\psi|^2$ is simplified:

$$|\psi|^2 = 1 - 8\sin\left(\frac{kdR}{r} - \pi\gamma\right)\sin\left[\frac{k(d-R)^2}{4r}\right]\cos\left[\frac{k(d+R)^2}{4r} - \pi\gamma\right].$$

The $|\psi|^2$ maxima for $\gamma = \frac{1}{2}$ are well separated from those for $\gamma = 0$. Thus, the measurement of the particle flux along the Z axis is realisable in practice. Using the properties of the Lommel functions one obtains for $(d+R)/r\sin\theta \ll 1$

$$\sigma_\gamma^T = \sigma_0^T + \left(\frac{1+\cos\theta}{\sin\theta}\right)^2 (d^2 - R^2)J_1[k(d+R)\sin\theta]$$

$$\times J[k(d-R)\sin\theta]\sin^2(\omega - \pi\gamma) \qquad (\omega = kdR/r).$$

Here σ_0^T is defined by (2.10). This cross section differs from the Fraunhöfer one (3.18) by the sine argument in the last term. This leads to ambiguities similar to those of two solenoids with $\phi_1 = -\phi_2$ (see section 4.4). It seems that the expressions presented describe adequately the experiments of Tonomura *et al* for the toroidal solenoid.

References

[1] Bawin M and Burnel A 1985 *J. Phys. A: Math. Gen.* **18** 2125
Peshkin M 1988 *Physica* B+C **151** 384

[2] Kamefuchi S (ed) 1984 *Proc. Int. Symp. on Foundations of Quantum Mechanics in the Light of New Technology* (Tokyo: Japanese Physical Society)

[3] Namiki M *et al* (eds) 1987 *Proc. 2nd Int. Symp. on Foundations of Quantum Mechanics in the Light of New Technology* (Tokyo: Japanese Physical Society)

[4] Loinger A 1987 *Riv. Nuovo Cimento* **10** 1

[5] Gorini V and Frigerio A (eds) 1986 *Fundamental Aspects of Quantum Theory* (New York: Plenum)

[6] Missiroli G F, Pozzi G and Valdre U 1981 *J. Phys. F: Sci. Instrum.* **14** 649
Möllenstedt G, Schmid H and Lichte H 1982 *Proc. Int. Congr. on Electron Microscopy, Hamburg* vol 1 (Frankfurt: Deutsche Gesellshaft fur Elektronentheorie e V) p 433

[7] Roy S M 1980 *Phys. Rev. Lett.* **44** 111

[8] Kobe D H and Liang D Q 1988 *Phys. Rev.* A **37** 1133

[9] Aharonov Y and Bohm D 1959 *Phys. Rev.* **115** 485

[10] Liang J Q 1986 *Nuovo Cimentio* B **92** 167
Liang J Q and Ding X X 1987 *Phys. Lett.* **119A** 325
Kobe D H and Liang J Q 1986 *Phys. Lett.* **118A** 475

[11] Tonomura A, Umezaki H, Matsuda T, Osakabe N, Endo J and Sugita Y 1984 *Proc. Int. Symp. on Foundations of Quantum Mechanics in the Light of New Technology* (Tokyo: Japanese Physical Society)

Tonomura A, Yano S, Osakabe N, Matsuda T, Yamada H, Kawasaki T and Endo J 1986 *Phys. Rev.* A **34** 815; 1987 *Proc. 2nd Int. Symp. on Foundations of Quantum Mechanics in the Light of New Technology* (Tokyo: Japanese Physical Society) pp 97–105
Tonomura A 1988 *Physica* B+C **151** 206
Peshkin M and Tonomura A 1989 *The Aharonov-Bohm Effect* (Berlin: Springer)
[12] Morandi G and Menossi E 1984 *Eur. J. Phys.* **5** 49
Liang J Q and Ding X X 1987 *Phys. Rev.* A **36** 4149
Schulman L 1971 *J. Math. Phys.* **12** 304
Inomata A 1987 *Proc. 2nd Int. Symp. on Foundations of Quantum Mechanics in the Light of New Technology* (Tokyo: Japanese Physical Society) pp 132–9
Liang J Q 1988 *Physica* B+C **151** 239
[13] Luboshitz V L and Smorodinsky J A 1978 *JINR preprint P2-11189*; *Sov. Phys.-JETP* **75** 40
[14] Afanasiev G N 1988 *J. Phys. A: Math. Gen.* **21** 2095
[15] Afanasiev G N 1988 *Nuovo Cimento* A **100** 967
[16] Sommerfeld A 1954 *Optics* (New York: Academic)
Bowcamp C J 1954 *Rep. Progr. Phys.* **17** 35
[17] Silver S 1962 *J. Opt. Soc. Am.* **52** 131
Hovenac E A 1989 *Am. J. Phys.* **57** 79
[18] Takabajasi T 1985 *Hadr. J. Suppl.* **1** 219
[19] Peshkin H, Talmie Y and Tassie L J 1961 *Ann. Phys., NY* **12** 426
[20] Tassie L J 1962 *Phys. Lett.* **5** 43
[21] Afanasiev G N 1988 *Vopr. At. Nauki Tech., Ser. Yad. Fyz.* **1** 49 (in Russian); *Nuovo Cimento* A **99** 647
[22] Dirac P A M 1931 *Proc. R. Soc.* A **133** 60
Berry M V 1980 *Eur. J. Phys.* **1** 240
[23] Landau L D and Lifschitz E M 1977 *Quantum Mechanics* (New York: Pergamon)
[24] Afanasiev G N 1987 *J. Comput. Phys.* **69** 196
[25] Dirac P A M 1958 *The Principles of Quantum Mechanics* (Oxford: Clarendon)
[26] Boyer T H 1987 *Nuovo Cimento* B **100** 685; *Phys. Rev.* A **36** 5083
[27] Comay E 1988 *Fizika* **20** 241
[28] Namiot V A 1987 *Phys. Lett.* **124** A 9
[29] Liang J Q 1988 *Physica* B+C **151** 239
[30] Honig W M, Kraft D W and Panarella E (eds) 1987 *Quantum Uncertainties. Recent and Future Experiments and interpretations* (New York: Plenum)